Chemical Science

ROYAL SOCIETY OF CHEMISTRY

EDGE ARTICLE

View Article Online
View Journal | View Issue

Cite this: *Chem. Sci.*, 2023, **14**, 4516

All publication charges for this article have been paid for by the Royal Society of Chemistry

Received 18th February 2023
Accepted 30th March 2023

DOI: 10.1039/d3sc00919j

rsc.li/chemical-science

Visible-light-induced chemo-, diastereo- and enantioselective α-C(sp^3)–H functionalization of alkyl silanes†

Lili Feng, Xiaofan Chen, Ning Guo, Yuqiao Zhou, Lili Lin, Weidi Cao* and Xiaoming Feng*

A catalytic asymmetric α-C(sp^3)–H functionalization of alkyl silanes with benzosultams was realized by merging photoredox and chiral Lewis acid catalysis. The key to success was the choice of photocatalyst with an appropriate redox potential and non-nucleophilic solvent, providing a novel entry to chiral organosilanes containing two adjacent tri- and tetra-substituted stereocenters with high to efficient diastereo- and enantioselectivity (up to 99% ee, 94 : 6 dr) under mild reaction conditions. Based on the control experiment and spectral analysis, an initial single electron transfer reduction of a benzosultam-triggered simultaneous or stepwise electron transfer/proton transfer process was proposed to rationalize the favored C(sp^3)–H functionalization rather than desilylation.

Introduction

The direct enantioselective functionalization of C(sp^3)–H is demonstrated to be an elegant, atom- and step-economic protocol to synthesize complex chiral molecules.[1–3] Thanks to the successive discovery of photocatalysts[4–7] in the past two decades, visible-light-promoted photocatalysis has emerged as a novel and powerful strategy for the purpose of formidable C(sp^3)–H activation regardless of the high bond dissociation energy,[8–12] which is complementary or even superior to that of the traditional transition metal-catalyzed C(sp^3)–H insertion or using an extra quantitative oxidant. In this context, several groups have accomplished photocatalytic asymmetric C(sp^3)–H functionalization of tertiary amines,[13–16] ethers,[17,18] sulfides,[18,19] hydrocarbons and their derivatives,[20–27] providing full and varied heteroatom-containing optically active compounds.

Organosilanes fulfill a plethora of roles in synthetic chemistry, and have potential applications in drug discovery due to the unique physicochemical characteristics of silicon.[28–30] We conceived that the direct photocatalytic asymmetric α-C(sp^3)–H functionalization of silanes would offer straightforward access to chiral silicon-containing compounds. To the best of our knowledge, organic silanes have served as sought-after alkyl radical precursors in photoredox reactions by exploiting the adequately lower oxidation potential than the parent arising from the higher σ–n or σ–π interactions.[31] Generally, the silanes undergo single electron transfer (SET) oxidation to form α-silyl cation radicals **A**, which are followed by C–Si bond or C–H bond cleavage to generate the desilylation radical species **B** or the α-

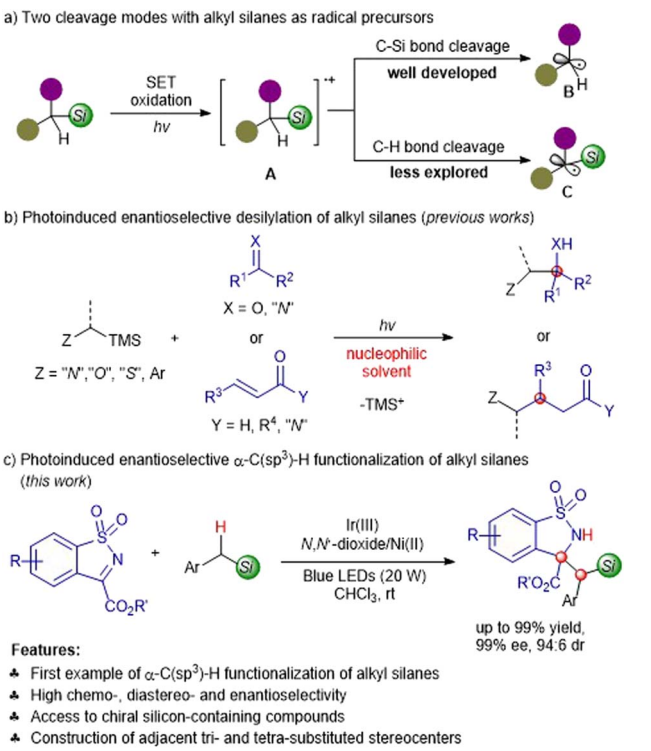

Scheme 1 Photoinduced asymmetric radical reactions with alkyl silanes as radical precursors.

Key Laboratory of Green Chemistry & Technology, Ministry of Education, College of Chemistry, Sichuan University, Chengdu 610064, China. E-mail: wdcao@scu.edu.cn; xmfeng@scu.edu.cn

† Electronic supplementary information (ESI) available: ^{1}H, ^{13}C{^{1}H} and ^{19}F{^{1}H} NMR, HPLC spectra, and CD spectra (PDF). X-ray crystallographic data for **3b**. CCDC 2117167. For ESI and crystallographic data in CIF or other electronic format see DOI: https://doi.org/10.1039/d3sc00919j

silyl radical species **C** (Scheme 1a).[32] The former producing non-silicon-containing products has been well developed in a variety of photoinduced enantioselective transformations (Scheme 1b);[33–45] by contrast, the latter has not been explored for the synthesis of chiral silicon-containing substances. The mechanistic studies reported by Mariano[32,46,47] and others[48,49] revealed that the generation of desilylation and silicon-containing products greatly depended on the photoreaction solvent, and the competitive desilylation dominants by means of a nucleophile-assisted C–Si bond cleavage with the solvent acting as the nucleophile. For example, Melchiorre and co-workers elegantly established the enantioselective β-alkylation of enals with alkyl silanes through MeCN-assisted C–Si bond fragmentation.[36,41] Herein, we reported the first visible-light-induced chemo-, diastereo- and enantioselective α-C(sp^3)–H functionalization of silanes with benzosultams under the Ir(III)/*N*,*N*′-dioxide-Ni(II) synergetic catalysis to produce enantioenriched silicon-containing compounds (Scheme 1c); the desilylation was suppressed *via* the ingenious choice of a suitable photocatalyst and non-nucleophilic solvent.

Results and discussion

At the beginning of this study, we selected the model reaction of benzosultam **1a** and benzyltrimethylsilane **2a** in $CHCl_3$. A variety of photocatalysts were investigated under the irradiation of blue LEDs (20 W) at room temperature with a **L_3-RaPr$_2$**/$Ni(OTf)_2$ complex as the chiral Lewis acid catalyst (Table 1, entries 1–3, see the ESI† for details). No reaction occurred by using photocatalyst Ru-1 (Table 1, entry 1). Delightedly, the reaction proceeded smoothly to afford the desired product **3a** in 69% yield, 63%/15% ee and 66 : 34 dr along with the formation of a trace amount of desilylation product **3a′** in the presence of Ir-1 (Table 1, entry 2). Nevertheless, the **3a′** obtained instead was catalyzed by Acr-1, which has a high exited state reduction potential (E_{red} ($^*Acr^+/Acr^\Sigma$) = +2.19 V *vs.* SCE in CH_3CN) (Table 1, entry 3).[50] The screening of chiral *N*,*N*′-dioxide ligands[51–61] showed that the sterically bulky **L_3-RaPr$_2$Ad** derived from 2,6-diisopropyl-4-adamantyl aniline promoted this reaction to give **3a** in 75% yield, 86 : 14 dr with 94% ee (Table 1, entry 4). Increasing the dosage of **1a** to 1.2 equiv. improved the yield to 94% with maintained diastereo- and enantioselectivity (Table 1, entry 5). The addition of a 4 Å molecular sieve (MS) raised the enantioselectivity slightly (95% ee, Table 1, entry 6). The solvent had an important influence on the chemoselectivity of this reaction. On switching $CHCl_3$ to nucleophilic solvents, such as CH_3OH, CH_3CN and THF, **3a′** was obtained without observation of **3a** (Table 1, entries 7–9), and the lower yield of **3a′** in THF was due to the competing α-C(sp^3)–H functionalization of THF with **1a** (Table 1, entry 9). Similarly, the reaction between toluene and

Table 1 Optimization of the reaction conditions[a]

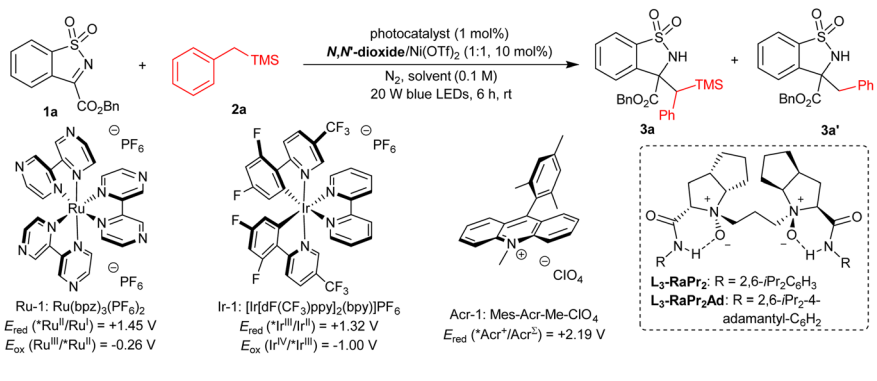

Entry	Photocatalyst	Ligand	Solvent	Yield of **3a**[b] (%)	ee of **3a**[b] (%)	dr (**3a**)[c]	Yield of **3a′**[c] (%)	ee of **3a′**[c] (%)
1	Ru-1	**L_3-RaPr$_2$**	$CHCl_3$	0	—	—	0	—
2	Ir-1	**L_3-RaPr$_2$**	$CHCl_3$	69	63/15	66 : 34	Trace	n. d.
3[d]	Acr-1	**L_3-RaPr$_2$**	$CHCl_3$	0	—	—	95	17
4	Ir-1	**L_3-RaPr$_2$Ad**	$CHCl_3$	75	94/47	86 : 14	Trace	n. d.
5[e]	Ir-1	**L_3-RaPr$_2$Ad**	$CHCl_3$	94	93/43	86 : 14	Trace	n. d.
6[e,f]	Ir-1	**L_3-RaPr$_2$Ad**	$CHCl_3$	95	95/43	86 : 14	Trace	n. d.
7[e]	Ir-1	**L_3-RaPr$_2$Ad**	CH_3OH	0	—	—	98	7
8[e]	Ir-1	**L_3-RaPr$_2$Ad**	CH_3CN	0	—	—	99	36
9[e]	Ir-1	**L_3-RaPr$_2$Ad**	THF	0	—	—	11	n. d.
10[e]	Ir-1	**L_3-RaPr$_2$Ad**	Toluene	23	92/35	85 : 15	75	47
11[e,g]	Ir-1	**L_3-RaPr$_2$Ad**	$CHCl_3$	0	—	—	0	—
12[e]	—	**L_3-RaPr$_2$Ad**	$CHCl_3$	0	—	—	0	—
13[e,h]	Ir-1	—	$CHCl_3$	48	—	52 : 48	0	—

[a] Unless otherwise noted, all the reactions were performed with a photocatalyst (1 mol%), $Ni(OTf)_2$ (10 mol%), ligand (10 mol%), **1a** (0.10 mmol) and **2a** (0.10 mmol) in solvent (1.0 mL) at room temperature under the irradiation of 20 W blue LEDs for 6 h. [b] Yield of the isolated product. [c] The ee and dr values were determined by UPCC analysis. [d] Acr-1 (2 mol%). [e] **1a** (0.12 mmol). [f] With 4 Å MS (20 mg), 0.5 h. [g] Without light. [h] In the absence of a **L_3-RaPr$_2$Ad**/Ni(II) complex. n. d. = not determined.

1a dominated with toluene as the solvent (Table 1, entry 10). Other reaction parameters were also examined, including a central metal salt, catalytic loading and so on, but no better result was achieved (see the ESI† for details). Additionally, control experiments were carried out to understand the synergic catalysis. No reaction occurred without light or a photocatalyst, proving the photochemical nature (Table 1, entries 11 and 12). Ir-1 could mediate this reaction itself, but afforded **3a** with 48% yield and 52 : 48 dr, implying that the **L_3-RaPr$_2$Ad**/Ni(OTf)$_2$ complex played a significant role in enhancing the reactivity and diastereoselectivity (Table 1, entry 13).

With the optimized reaction conditions in hand (Table 1, entry 6), the substrate scope was then evaluated. As shown in Scheme 2, on changing the benzyl ester of benzosultams to a methyl ester (**1b**) and ethyl ester (**1c**), the corresponding products **3b**[62] (96% ee, 83 : 17 dr) and **3c** (90% ee, 86 : 14 dr) were obtained smoothly. With respect to the substituents on the phenyl group, the reaction of **1f–1i** bearing an electron-withdrawing group afforded **3f–3i** with excellent enantioselectivities (96–99% ee), which was superior to that of electron-rich ones (**3d-3e**, 84–88% ee). An imine containing fused naphthyl motif was also tolerated but provided **3j** in only 30% yield, 82% ee and 80 : 20 dr. Next, we turned our attention to the scope of silanes. Various substituted benzyl trimethylsilanes were applicable in this synergistic catalytic system to afford the α-C(sp^3)–H functionalization products **3k–3s.** Both the electrical properties and position of the substituents have obvious effects on this reaction. The silanes bearing electron-donating groups

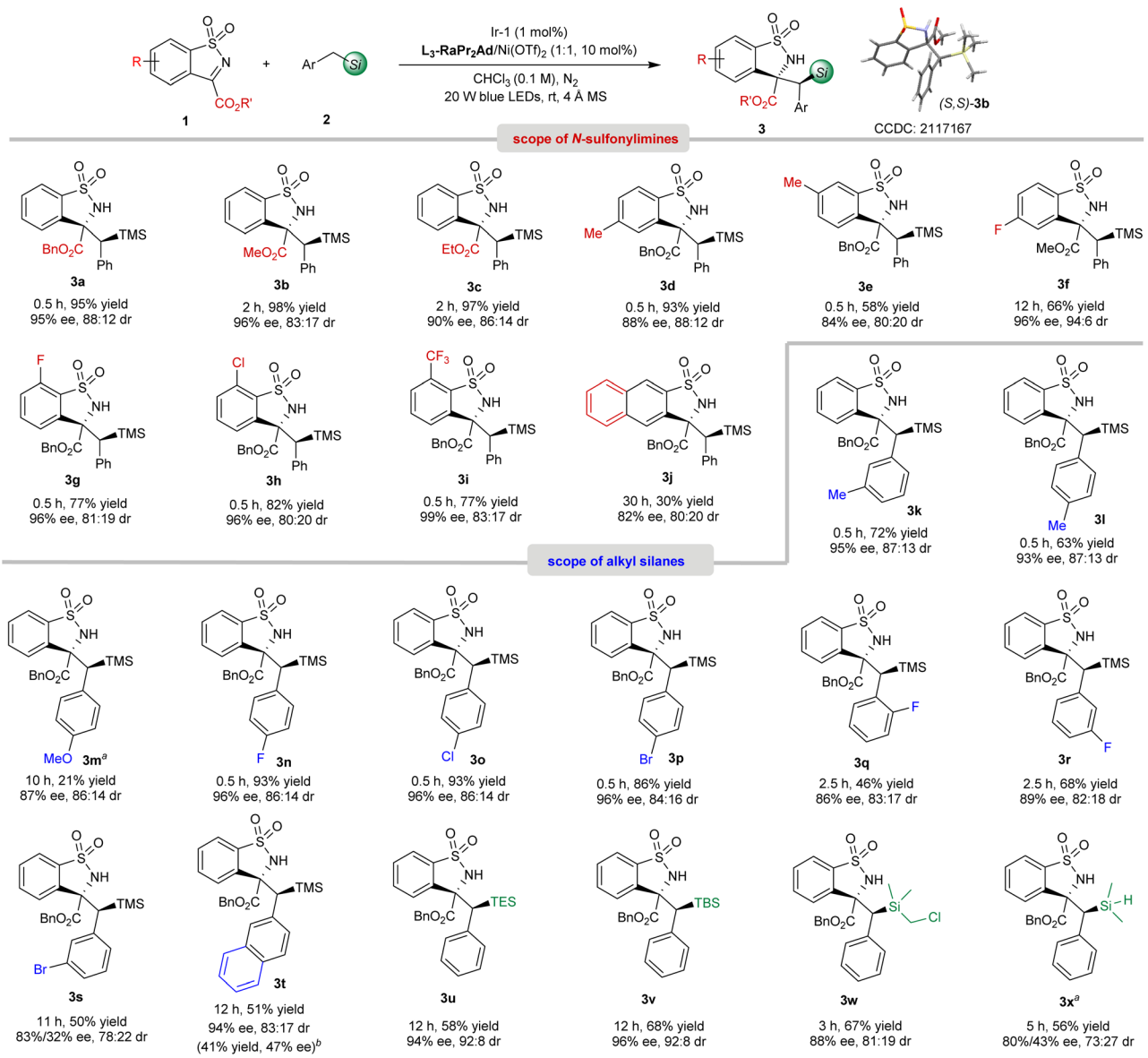

Scheme 2 The substrate scope. Reaction conditions: Ir-1 (1 mol%), Ni(OTf)$_2$/**L_3-RaPr$_2$Ad** (1 : 1, 10 mol%), **1** (0.12 mmol), **2** (0.10 mmol), and 4 Å MS (20 mg) in $CHCl_3$ (1.0 mL) at rt under the irradiation of 20 W blue LEDs for the indicated time. Yield of the isolated product, and the dr value was determined by ^{1}H NMR spectroscopy and ee value was analyzed by UPCC with a chiral column. [a]$[Ir[dF(CF_3)ppy]_2(dtbbpy)]PF_6$ (1 mol%) instead. [b]The data of desilylation product **3t′** are given in parenthesis.

at the *para*-position of the phenyl group exhibited lower reactivity and stereoselectivity. For example, salines containing halo-substituents at the *para*-position, gave **3n–3p** with 86–93% yield and 96% ee, while *para*-methyl and *para*-methoxyl benzyl substituted **3l-3m** were obtained in 21–63% yield with lower enantioselectivity (87–93% ee). If the electron-withdrawing groups were located at the *ortho*- or *meta*-positions, decreased reactivity and stereoselectivity were observed (**3q–3s**, 46–68% yield, 83–89% ee, and 78 : 22–83 : 17 dr). Noteworthily, regioselective secondary C(sp^3)–H functionalization adjacent to the silicon atom took place to afford **3k-3l** solely without observation of the primary C(sp^3)–H bond fragmentation. Trimethyl(naphthalen-2-ylmethyl)silane reacted with **1a** to deliver **3t** in 51% yield and 94% ee with 83 : 17 dr, and the desilylation product **3t′** was also isolated in 41% yield with 47% ee. Benzyltriethylsilane (BnTES), benzylic dimethyl tert-butylsilane (BnTBS), $BnSiMe_2CH_2Cl$ and $BnSiMe_2H$ were also suitable substrates, successfully generating **3u–3x** with 56–68% yield, 80–96% ee and 73 : 27–92 : 8 dr. It was worth mentioning that no Si–H bond cleavage product through a silyl radical intermediate was observed.[63]

To get insight into the reaction process, a series of mechanistic studies were conducted. The reaction was completely inhibited with the addition of 2,2,6,6-tetramethylpiperidine-1-oxyl (see the ESI† for details). The Stern–Volmer fluorescence quenching experiments unambiguously showed that **1a** quenched Ir-1 effectively, but **2a** has no obvious quenching effect (Scheme 3a). Moreover, **1a** underwent homocoupling to give the product **4a** with 26% yield in the presence of Ir-1 (0.5 equiv.), while no reaction of **2a** occurred (Scheme 3b). The observation was consistent with the redox potential between Ir-1 and **1a** or **2a** (Scheme 3b). The electron paramagnetic resonance (EPR) measurement was also performed with 5,5-dimethyl-1-pyrroline *N*-oxide (DMPO) as a trapping agent. It witnessed the formation of the persistent radical **6** (g = 2.0066, AN = 12.91 G, and AH = 10.40 G) through EPR simulation (Scheme 3c),[64] which was further conformed based on the detection of **6** by using the high resolution mass spectrum (HRMS) (Scheme 3c). These results strongly indicated that Ir-1 underwent oxidative quenching to trigger the generation of a radical anion $\mathbf{1a}^{\bullet-}$ from imine. In addition, deuterated experiments revealed that the proton source of the N–H bond in

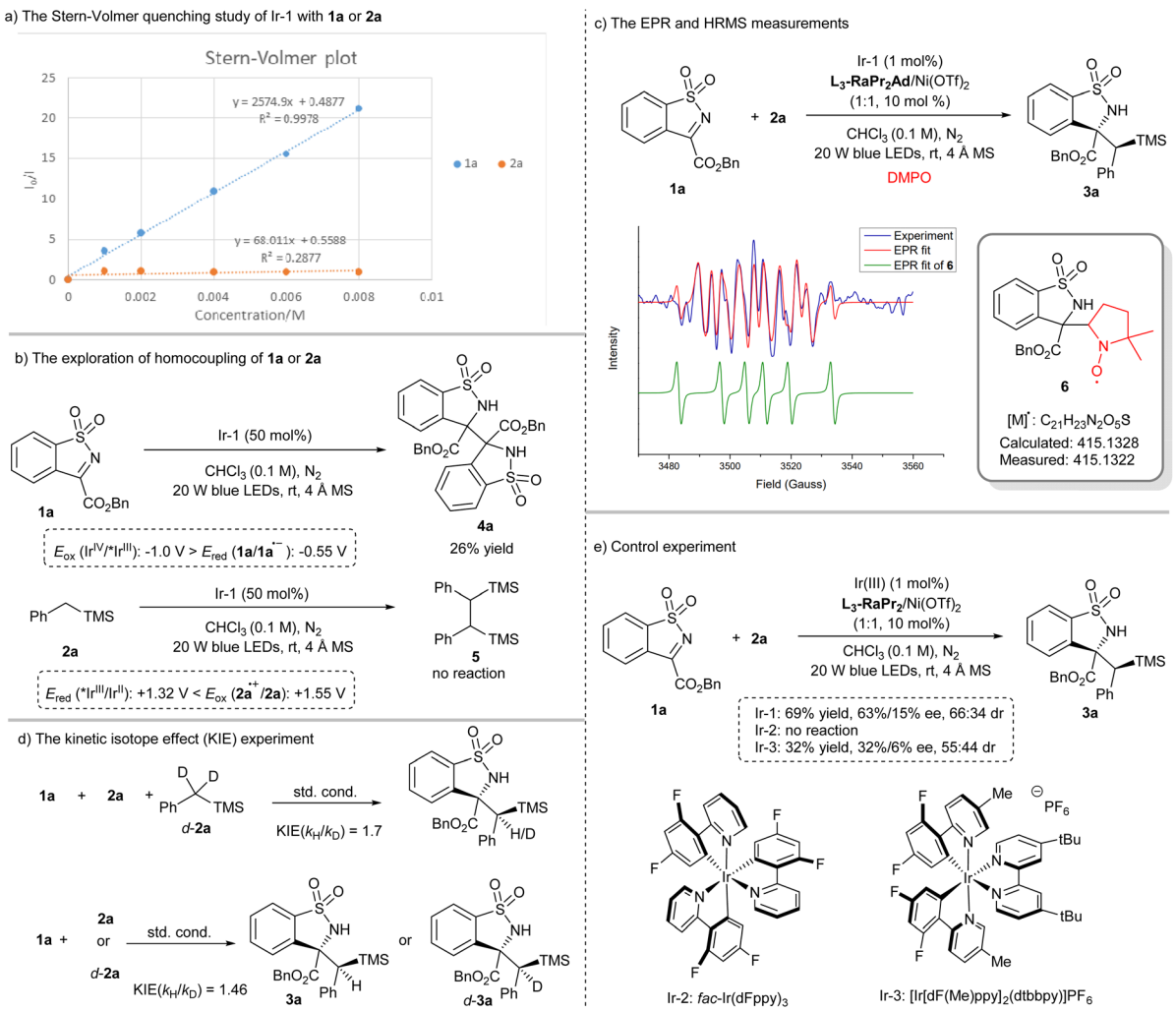

Scheme 3 The mechanistic studies.

3a came from **1a** (see the ESI† for details), and a primary kinetic isotope effect (KIE) of about 1.7 and 1.47 for the competitive and parallel experiments revealed that the C(sp^3)–H bond cleavage may be involved in the rate-limiting step (Scheme 3d). Next, the pathway of C(sp^3)–H bond cleavage of alkyl silane was clarified: direct hydrogen atom transfer (HAT), electron transfer (ET)/proton transfer (PT) sequence or multisite proton-coupled electron transfer (MS-PCET)[65–68] (see the ESI† for details)? Firstly, the photocatalysts Ir-1 and Ir-2 possessed the same triplet state energy (60.1 kcal mol^{-1});[69] however, the latter could not facilitate this reaction (Scheme 3e), and the result was consistent with the observation of the formation of **3x** rather than the Si–H bond cleavage product,[63] which might exclude the direct HAT between **2a** and triplet state **1a** that was formed through energy transfer. Secondly, the reactions between **1a** and THF or toluene proceeded smoothly (Table 1, entries 9 and 10) although the oxidation potentials of THF (>+2.4 V *vs.* SCE in CH_3CN) and toluene (+2.26 V *vs.* SCE in CH_3CN) are much higher than that of the Ir-1 ($E_{ox}(Ir^{IV/III})$ = +1.69 V *vs.* SCE in CH_3CN). Moreover, Ir-3 could mediate this reaction to give **3a** with 32% yield (Scheme 3e), but the potential was also mismatched between Ir-3 (E_{red} ($^*Ir^{III}/Ir^{II}$) = +0.75 V, E_{ox} (Ir^{IV}/Ir^{III}) = +1.49 V *vs.* SCE in CH_3CN) and **2a** (E_{ox} ($\mathbf{2a}^{\bullet+}/\mathbf{2a}$) = +1.55 V *vs.* SCE in CH_3CN, see the ESI† for details). Thus, a SET reduction of imine followed by the MS-PCET mechanism was surmised. However, **3a′** was obtained exclusively in nucleophilic solvents (Table 1, entries 7–9), indicating the existence of radical cation $\mathbf{2a}^{\bullet+}$ generated through SET oxidation of **2a** by Ir-1(IV), which meant that the stepwise ET/PT may be also involved. In addition, the quantum yield was found to be 0.23, suggesting that a radical chain propagation in this reaction may not be the predominant process.

According to above experimental results, the catalytic cycle was proposed as shown in Fig. 1. The **L_3-RaPr$_2$Ad**/$Ni(OTf)_2$ complex coordinated with **1a** to form the intermediate **I**, which underwent SET reduction with the photocatalyst [Ir^{III}] under visible-light illumination and afforded the radical anion **II**; accordingly, [Ir^{III}] went through oxidative quenching to form the [Ir^{IV}] species. The following C–H bond cleavage of **2a** through MS-PCET involving electron transfer to [Ir^{IV}] (oxidant) and proton transfer to **II** (base)[70] regenerated [Ir^{III}] and produced a radical–radical pair **III** (path a). Alternatively, **III** was formed through a stepwise process, namely, SET between **2a** and [Ir^{IV}] took place to afford the radical cation **IV**, followed by proton transfer to **II** (path b). Subsequently, **III** underwent stereocontrolled radical coupling to provide **3a**. Additionally, an unproductive homocoupling of **II** proceeded to yield the byproduct **4a**.

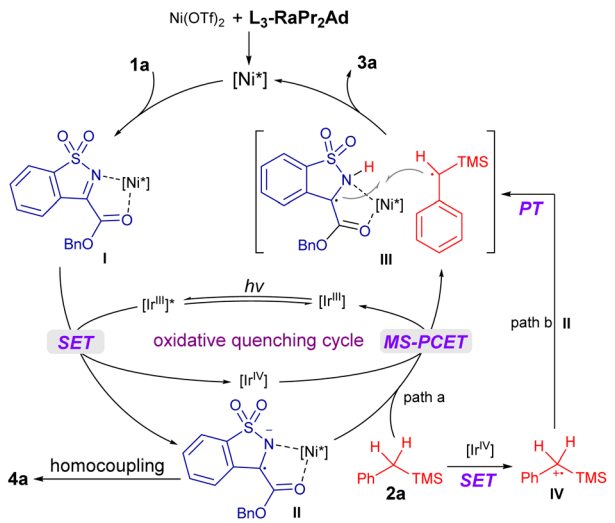

Fig. 1 The proposed catalytic cycle.

Conclusions

In summary, a bimetallic synergetic photocatalytic chemo-, diastereo- and enantioselective α-C(sp^3)–H functionalization of alkyl silanes with benzosultams was discovered. Diverse experimental evidence revealed that the Ir(III) photocatalyst underwent an oxidative quenching cycle to facilitate SET reduction of benzosultam and afforded a radical anion. It triggered the following MS-PCET or stepwise ET/PT of alkyl silanes and radical coupling. This protocol provided a rapid and facile access to chiral organosilanes containing two adjacent tri- and tetra-substituted stereocenters with good to excellent yield and stereoselectivities. The extension of this methodology to synthesize chiral silanes is underway in our laboratory.

Data availability

Further details of experimental procedure, ^1H, $^{13}C\{^1H\}$ and $^{19}F\{^1H\}$ NMR, HPLC, CD spectra, X-ray crystallographic data for 3b are available in the ESI.†

Author contributions

L. L. F. preformed the experiments. X. F. C. repeated the data. N. G. participated in the synthesis of substrates and ligands. X. M. F., L. L. L. and W. D. C. supervised the project. W. D. C. and L. L. F. co-wrote the manuscript. Y. Q. Z. performed the X-ray single crystal diffraction analysis.

Conflicts of interest

There are no conflicts to declare.

Acknowledgements

We acknowledge the National Natural Science Foundation of China (no. 22188101, 22071160 and 92256302), and Sichuan Science and Technology Program (no. 2021YJ0562) for financial support. We thank Dr Hanjiao Chen (Sichuan University) for the assistance with the EPR experiment.

Notes and references

1 C. G. Newton, S. G. Wang and C. C. Oliveira, *Chem. Rev.*, 2017, **117**, 8908–8976.

2 T. G. Saint-Denis, R. Y. Zhu, G. Chen, Q. F. Wu and J. Q. Yu, *Science*, 2018, **359**, eaao4798.
3 Q. Zhang and B. F. Shi, *Chin. J. Chem.*, 2019, **37**, 647–656.
4 C. K. Prier, D. A. Rankic and D. W. C. MacMillan, *Chem. Rev.*, 2013, **113**, 5322–5363.
5 N. A. Romero and D. A. Nicewicz, *Chem. Rev.*, 2016, **116**, 10075–10166.
6 M. J. Genzink, J. B. Kidd, W. B. Swords and T. P. Yoon, *Chem. Rev.*, 2022, **122**, 1654–1716.
7 Y. Wu, D. Kim and T. S. Teets, *Synlett*, 2022, **33**, 1154–1179.
8 L. Shi and W. Xia, *Chem. Soc. Rev.*, 2012, **41**, 7687–7697.
9 Q. Qin, H. Jiang, Z. Hu, D. Ren and S. Yu, *Chem. Rec.*, 2017, **17**, 754–774.
10 L. Revathi, L. Ravindar, W. Y. Fang, K. P. Rakesh and H. L. Qin, *Adv. Synth. Catal.*, 2018, **360**, 4652–4698.
11 M. Uygur and O. G. Mancheño, *Org. Biomol. Chem.*, 2019, **17**, 5475–5489.
12 N. Holmberg-Douglas and D. A. Nicewicz, *Chem. Rev.*, 2022, **122**, 1925–2016.
13 D. Uraguchi, N. Kinoshita, T. Kizu and T. Ooi, *J. Am. Chem. Soc.*, 2015, **137**, 13768–13771.
14 C. Wang, J. Qin, X. Shen, R. Riedel, K. Harms and E. Meggers, *Angew. Chem., Int. Ed.*, 2016, **55**, 685–688.
15 J. J. Murphy, D. Bastida, S. Paria, M. Fagnoni and P. Melchiorre, *Nature*, 2016, **532**, 218–222.
16 T. Y. Zhan, L. K. Yang, Q. Y. Chen, R. Weng, X. H. Liu and X. M. Feng, *CCS Chem.*, 2022, **4**, DOI: **10.31635/ccschem.022.202202405**.
17 C. Wang, K. Harms and E. Meggers, *Angew. Chem., Int. Ed.*, 2016, **55**, 13495–13498.
18 Z. D. Tan, S. B. Zhu, Y. B. Liu and X. M. Feng, *Angew. Chem., Int. Ed.*, 2022, **61**, e202203374.
19 W. Yuan, Z. Zhou, L. Gong and E. Meggers, *Chem. Commun.*, 2017, **53**, 8964–8967.
20 D. Mazzarella, G. E. Crisenza and P. Melchiorre, *J. Am. Chem. Soc.*, 2018, **140**, 8439–8443.
21 Y. Li, M. Lei and L. Gong, *Nat. Catal.*, 2019, **2**, 1016–1026.
22 H. Mitsunuma, S. Tanabe, H. Fuse, K. Ohkubo and M. Kanai, *Chem. Sci.*, 2019, **10**, 3459–3465.
23 Z. Y. Dai, Z. S. Nong and P. S. Wang, *ACS Catal.*, 2020, **10**, 4786–4790.
24 S. Cao, W. Hong, Z. Ye and L. Gong, *Nat. Commun.*, 2021, **12**, 2377.
25 J. Kikuchi, S. Kodama and M. Terada, *Org. Chem. Front.*, 2021, **8**, 4153–4159.
26 Z. Y. Dai, Z. S. Nong, S. Song and P. S. Wang, *Org. Lett.*, 2021, **23**, 3157–3161.
27 H. Yu, T. Zhan, Y. Zhou, L. Chen, X. H. Liu and X. M. Feng, *ACS Catal.*, 2022, **12**, 5136–5144.
28 A. K. Franz and S. O. Wilson, *J. Med. Chem.*, 2013, **56**, 388–405.
29 E. Rémond, C. Martin, J. Martinez and F. Cavelier, *Chem. Rev.*, 2016, **116**, 11654–11684.
30 S. J. Barraza and S. E. Denmark, *J. Am. Chem. Soc.*, 2018, **140**, 6668–6684.
31 J. I. Yoshida, K. Kataoka, R. Horcajada and A. Nagaki, *Chem. Rev.*, 2008, **108**, 2265–2299.
32 E. Hasegawa, W. Xu, P. S. Mariano, U.-C. Yoon and J.-U. Kim, *J. Am. Chem. Soc.*, 1988, **110**, 8099–8111.
33 L. Ruiz Espelt, I. S. McPherson, E. M. Wiensch and T. P. Yoon, *J. Am. Chem. Soc.*, 2015, **137**, 2452–2455.
34 J. Ma, K. Harms and E. Meggers, *Chem. Commun.*, 2016, **52**, 10183–10186.
35 T. Kizu, D. Uraguchi and T. Ooi, *J. Org. Chem.*, 2016, **81**, 6953–6958.
36 M. Silvi, C. Verrier, Y. P. Rey, L. Buzzetti and P. Melchiorre, *Nat. Chem.*, 2017, **9**, 868–873.
37 Z. Y. Cao, T. Ghosh and P. Melchiorre, *Nat. Commun.*, 2018, **9**, 3274.
38 X. Shen, Y. Li, Z. Wen, S. Cao, X. Hou and L. Gong, *Chem. Sci.*, 2018, **9**, 4562–4568.
39 B. Han, Y. Li, Y. Yu and L. Gong, *Nat. Commun.*, 2019, **10**, 3804.
40 S. K. Pagire, N. Kumagai and M. Shibasaki, *Chem. Sci.*, 2020, **11**, 5168–5174.
41 E. Le Saux, D. Ma, P. Bonilla, C. M. Holden, D. Lustosa and P. Melchiorre, *Angew. Chem., Int. Ed.*, 2021, **60**, 5357–5362.
42 X. Dong, Q. Y. Li and T. P. Yoon, *Org. Lett.*, 2021, **23**, 5703–5708.
43 J. Y. Kim, Y. S. Lee and D. H. Ryu, *ACS Catal.*, 2021, **11**, 14811–14818.
44 S. M. Cho, J. Y. Kim, S. Han and D. H. Ryu, *J. Org. Chem.*, 2022, **87**, 11196–11203.
45 L. Z. Hou, Y. Q. Zhou, H. Yu, T. Y. Zhan, W. D. Cao and X. M. Feng, *J. Am. Chem. Soc.*, 2022, **144**, 22140–22149.
46 U.-C. Yoon and P. S. Mariano, *Acc. Chem. Res.*, 1992, **25**, 233–240.
47 U. C. Yoon, P. S. Mariano, L. Cermenati, M. Freccero, P. Venturello and A. Albini, *J. Am. Chem. Soc.*, 1995, **117**, 7869–7876.
48 J. P. Dinnocenzo, S. Farid, J. L. Goodman, I. R. Gould, S. L. Mattes and W. P. Todd, *J. Am. Chem. Soc.*, 1989, **111**, 8973–8975.
49 K. P. Dockery, J. P. Dinnocenzo, S. Farid, J. L. Goodman, I. R. Gould and W. P. Todd, *J. Am. Chem. Soc.*, 1997, **119**, 1876–1883.
50 **3a′** was obtained instead probably due to the initial SET oxidation of **2a** rather than SET reduction of **1a** with exited state Acr-1. A benzyl radical cation was formed and it released a TMS+ group preferentially because no suitable base (*e.g.* radical anion **II** in Fig. 1) accepted the proton, leading to the generation of a benzyl radical, which underwent radical addition to **1a** and SET/protonation to produce **3a′**. See the ESI† for the possible catalytic cycle with Acr-1 as the catalyst.
51 X. H. Liu, L. L. Lin and X. M. Feng, *Acc. Chem. Res.*, 2011, **44**, 574–587.
52 X. H. Liu, L. L. Lin and X. M. Feng, *Org. Chem. Front.*, 2014, **1**, 298–302.
53 X. H. Liu, H. F. Zheng, Y. Xia, L. L. Lin and X. M. Feng, *Acc. Chem. Res.*, 2017, **50**, 2621–2631.
54 X. H. Liu, S. X. Dong, L. L. Lin and X. M. Feng, *Chin. J. Chem.*, 2018, **36**, 791–797.
55 M.-Y. Wang and W. Li, *Chin. J. Chem.*, 2021, **39**, 969–984.

56 S. X. Dong, X. H. Liu and X. M. Feng, *Acc. Chem. Res.*, 2022, **55**, 415–428.
57 Y. H. Wen, X. Huang and X. M. Feng, *Synlett*, 2005, 2445–2448.
58 X. Zhang, D. H. Chen, X. H. Liu and X. M. Feng, *J. Org. Chem.*, 2007, **72**, 5227–5233.
59 L. Dai, W. Liu, Y. Q. Zhou, Z. Zeng, X. Y. Hu, W. D. Cao and X. M. Feng, *Angew. Chem., Int. Ed.*, 2021, **60**, 26599–26603.
60 Q. W. He, D. Zhang, F. C. Zhang, X. H. Liu and X. M. Feng, *Org. Lett.*, 2021, **23**, 6961–6966.
61 D. Zhang, M. P. Pu, Z. Z. Liu, Y. Q. Zhou, Z. D. Yang, X. H. Liu, Y.-D. Wu and X. M. Feng, *J. Am. Chem. Soc.*, 2023, **145**, 4808–4818.
62 CCDC 2117167 (**3b**).
63 X. Fan, P. Xiao, Z. Jiao, T. Yang, X. Dai, W. Xu, J. D. Tan, G. Cui, H. Su, W. Fang and J. Wu, *Angew. Chem., Int. Ed.*, 2019, **58**, 12580–12584.
64 G. R. Buettner, *Free Radical Biol. Med.*, 1987, **3**, 259–303.
65 E. C. Gentry and R. R. Knowles, *Acc. Chem. Res.*, 2016, **49**, 1546–1556.
66 Z. Zhou, X. Kong and T. Liu, *Chin. J. Org. Chem.*, 2021, **41**, 3844–3879.
67 R. G. Agarwal, S. C. Coste, B. D. Groff, A. M. Heuer, H. Noh, G. A. Parada, C. F. Wise, E. M. Nichols, J. J. Warren and J. M. Mayer, *Chem. Rev.*, 2022, **122**, 1–49.
68 P. R. D. Murray, J. H. Cox, N. D. Chiappini, C. B. Roos, E. A. McLoughlin, B. G. Hejna, S. T. Nguyen, H. H. Ripberger, J. M. Ganley, E. Tsui, N. Y. Shin, B. Koronkiewicz, G. Qiu and R. R. Knowles, *Chem. Rev.*, 2022, **122**, 2017–2291.
69 A. Singh, K. Teegardin, M. Kelly, K. S. Prasad, S. Krishnan and J. D. Weaver, *J. Organomet. Chem.*, 2015, **776**, 51–59.
70 C. M. Morton, Q. Zhu, H. Ripberger, L. Troian-Gautier, Z. S. D. Toa, R. R. Knowles and E. J. Alexanian, *J. Am. Chem. Soc.*, 2019, **141**, 13253–13260.